Cell

CRTAP Is Required for Prolyl 3-Hydroxylation and Mutations Cause Recessive Osteogenesis Imperfecta

Roy Morello,[1] Terry K. Bertin,[1] Yuqing Chen,[1,11] John Hicks,[2] Laura Tonachini,[3] Massimiliano Monticone,[3] Patrizio Castagnola,[3] Frank Rauch,[4,5] Francis H. Glorieux,[4,5] Janice Vranka,[6,7] Hans Peter Bächinger,[6,7] James M. Pace,[8] Ulrike Schwarze,[8] Peter H. Byers,[8] MaryAnn Weis,[9] Russell J. Fernandes,[9] David R. Eyre,[9] Zhenqiang Yao,[10] Brendan F. Boyce,[10] and Brendan Lee[1,11,12,*]

[1] Department of Molecular and Human Genetics
[2] Department of Pathology, Texas Children's Hospital
Baylor College of Medicine, Houston, TX 77030, USA
[3] Istituto Nazionale per la Ricerca sul Cancro, Genova, Italy
[4] Genetics Unit, Shriners Hospital for Children, Montreal, Canada
[5] McGill University, Montreal, Canada
[6] Shriners Hospital for Children, Portland, OR 97201, USA
[7] Department of Biochemistry and Molecular Biology, Oregon Health & Science University, OR 97239, USA
[8] Department of Pathology
[9] Department of Orthopaedics and Sports Medicine
University of Washington, Seattle, WA 98195, USA
[10] Department of Pathology and Laboratory Medicine, University of Rochester Medical Center, Rochester, NY 14627, USA
[11] Howard Hughes Medical Institute, Houston, TX 77030, USA
[12] One Baylor Plaza, Room 635E, Houston, TX 77030, USA
*Contact: blee@bcm.tmc.edu
DOI 10.1016/j.cell.2006.08.039

SUMMARY

Prolyl hydroxylation is a critical posttranslational modification that affects structure, function, and turnover of target proteins. Prolyl 3-hydroxylation occurs at only one position in the triple-helical domain of fibrillar collagen chains, and its biological significance is unknown. CRTAP shares homology with a family of putative prolyl 3-hydroxylases (P3Hs), but it does not contain their common dioxygenase domain. Loss of *Crtap* in mice causes an osteochondrodysplasia characterized by severe osteoporosis and decreased osteoid production. CRTAP can form a complex with P3H1 and cyclophilin B (CYPB), and *Crtap*−/− bone and cartilage collagens show decreased prolyl 3-hydroxylation. Moreover, mutant collagen shows evidence of overmodification, and collagen fibrils in mutant skin have increased diameter consistent with altered fibrillogenesis. In humans, *CRTAP* mutations are associated with the clinical spectrum of recessive osteogenesis imperfecta, including the type II and VII forms. Hence, dysregulation of prolyl 3-hydroxylation is a mechanism for connective tissue disease.

INTRODUCTION

Collagens and proteins with collagenous domains constitute a large superfamily characterized by the unique repeating Gly-X-Y motif that is required for the formation of a triple-helical tertiary structure and in which Y is often 4-hydroxyproline (Eyre, 2004; Myllyharju and Kivirikko, 2004). The fibril-forming collagens (types I, II, III, V, and XI) are an important group characterized by a continuous triple helical domain that extends for more than 1000 amino acids. Mutations in the fibrillar collagen genes were among the first identified to cause osteodysplasias, i.e., osteogenesis imperfecta (OI), due to *COL1A1* and *COL1A2* mutations (Pihlajaniemi et al., 1984), and chondrodysplasias, i.e., the spondyloepiphyseal dysplasia spectrum, due to *COL2A1* mutations (Dreyer et al., 1998; Lee et al., 1989). Mutations in these genes result either in quantitative deficiencies or sequence alterations leading to structural defects of the triple helix, altered secretion, and abnormal fibril formation and/or assembly (Byers and Cole, 2002). More recently, defects in the posttranslational modification machinery of collagens have been associated with other disorders, e.g., Ehlers Danlos syndrome type VI (Hyland et al., 1992).

Nascent procollagen α chains undergo extensive posttranslational modification on entry into the rough endoplasmic reticulum (rER) (Lamande and Bateman, 1999; Myllyharju and Kivirikko, 2004). Enzymatic modifications include prolyl 4-hydroxylation, prolyl 3-hydroxylation, lysyl hydroxylation, and glycosylation by collagen

glucosyl/galactosyl-transferase. The hydroxylating reactions are mediated by enzymes containing the catalytic 2-oxoglutarate and Fe(II)-dependent dioxygenase domain. These enzymes require Fe(II), 2-oxoglutarate, molecular oxygen (O_2), and ascorbate to oxidatively decarboxylate 2-oxoglutarate to form succinate (Aravind and Koonin, 2001). One atom of oxygen from molecular O_2 is then transferred to succinate, while the other is used to hydroxylate the protein substrate. Hydroxylation reactions affect not only the thermal and structural stability of extracellular collagens but also, for instance, the turnover of proteins such as the hypoxia inducible factor (HIF) (Semenza, 2001). Collagen prolyl 4-hydroxylation occurs in the endoplasmic reticulum and is mediated by a tetrameric prolyl 4-hydroxylase (P4H) complex (Myllyharju, 2003). Almost complete 4-hydroxylation of all prolines in the Y position is necessary for fibrillar collagen stability at 37°C (Berg and Prockop, 1973a; Berg and Prockop, 1973b). Moreover, this modification is found in over 30 additional proteins with collagen domains.

The functional consequences of prolyl 3-hydroxylation of collagens are less understood. 3-Hyp occurs at the X position in Gly-X-Y triplets and is most abundant in type IV collagen where there are 10–15 residues per 1000 amino acids of the triple-helical domain (Kefalides, 1973; Kresina and Miller, 1979). In contrast, the fibrillar types I and II collagens have only one 3-Hyp residue per α1 chain (Kefalides, 1973). This raises the possibility that 3-Hyp may serve divergent functions in fibrillar versus network collagens. Biophysical studies of synthetic Gly-3-Hyp-Pro polypeptides suggest that 3-Hyp can destabilize the triple helix in contrast to the stabilizing effect of 4-Hyp (Jenkins et al., 2003; Mizuno et al., 2004).

A family of genes that encode for proteins with collagen prolyl 3-hydroxylase (P3H) activity, including P3H1 (Leprecan), has been recently reported (Vranka et al., 2004). Leprecan was originally described as a putative basement membrane-associated proteoglycan (Wassenhove-McCarthy and McCarthy, 1999), and subsequently, as a potential growth suppressor gene on chromosome 1, GROS1 (Kaul et al., 2000). It shares the catalytic dioxygenase domain found in collagen prolyl 4-hydroxylases and lysyl hydroxylases.

In a differential expression screen of hypertrophic versus proliferating chick embryo chondrocytes, we isolated a cDNA coding for cartilage associated protein (CASP or CRTAP) (Castagnola et al., 1997; Morello et al., 1999; Tonachini et al., 1999). This protein is characterized by a signal peptide and a tetratricopeptide-like helical domain (Andrade et al., 2001), which share high similarity with the amino-terminal half of Leprecan. CRTAP copurifies with protein fractions containing P3H activity but does not share the enzymatically active domain (Vranka et al., 2004).

Osteogenesis imperfecta is a major cause of brittle bone disease. The clinical spectrum of severe to mild OI is described by clinical types II, III, IV, and I. Until now, OI has been shown to be caused only by mutations in the type I collagen genes, *COL1A1* and *COL1A2* (Byers and Cole, 2002). However, newly defined types of OI, including types V, VI, and VII, have suggested increasing genetic heterogeneity, but candidate genes have not yet been identified (Glorieux et al., 2000; Glorieux et al., 2002; Ward et al., 2002).

In this study, we show that *Crtap* null mice have chondro-osseous dysplasia with rhizomelia, kyphosis, and severe osteopenia. At a biochemical level, they lack fibrillar collagen prolyl 3-hydroxylation, suggesting an essential role in the hydroxylation of specific prolyl residues and an interaction between CRTAP and P3H1. We further show that in humans, *CRTAP* mutations cause recessive OI, ranging from neonatal lethal cases (OI type II) to a milder phenotype (OI type VII) depending upon the nature of mutation.

RESULTS

Crtap Is Expressed in the Skeleton, and Loss of Its Function Causes an Osteochondrodysplasia with Severe Osteopenia

On Northern analysis, *Crtap* is expressed in most tissues to varying degrees (Morello et al., 1999). By mRNA in situ hybridization (ISH), it is highly expressed in growth-plate proliferating chondrocytes and in cells at the chondro-osseous junction (Figures 1A and 1B). At E15.5, it is expressed strongly in the presumptive bone collar of the diaphyses, where vascular and osteoblast invasion is initiated (Figure 1A, arrow). Its expression is low in hypertrophic chondrocytes (Figures 1A and 1C, arrowhead), and RT-PCR analysis confirmed expression in both osteoblasts and osteoclasts (Figure 1H). Immunohistochemical analyses using two different anti-CRTAP rabbit antisera displayed identical staining patterns and confirmed the distribution seen by ISH. Most of the CRTAP protein is located within the cells, although some signal is detected in the extracellular matrix (Figure 1C).

To determine the in vivo function of *Crtap*, we generated *Crtap* mutant mice by homologous recombination (Figures 1D–1F). Northern analysis of whole embryo RNA as well as RT-PCR of mutant osteoblast RNA confirmed absence of *Crtap* mRNA in mutant mice (Figure 1G). *Crtap* null mice are born at the expected Mendelian ratios, and they develop progressive and severe kyphoscoliosis over the first 6 months of age (Figures 2A and 2B). Moreover, they exhibit prenatal and postnatal growth delay that is characterized by shortening of long bone segments, affecting in particular the proximal segment of the limb. The ratio between femoral versus tibial lengths in mutant versus wild-type (WT) mice is consistent with rhizomelia (WT = 0.82 ± 0.014; mutant = 0.77 ± 0.018; N = 6 each group; $p < 0.01$; Figures 2C and 2D). The growth plate shows slightly disorganized growth columns of proliferating chondrocytes with areas of focal cell drop out, while the zone of hypertrophy remains fairly intact (Figure 2F).

Skeletal radiographs and Von Kossa-stained calcified bone sections showed striking evidence of osteoporosis (Figures 2D and 2E). Mutant mice have decreased bone

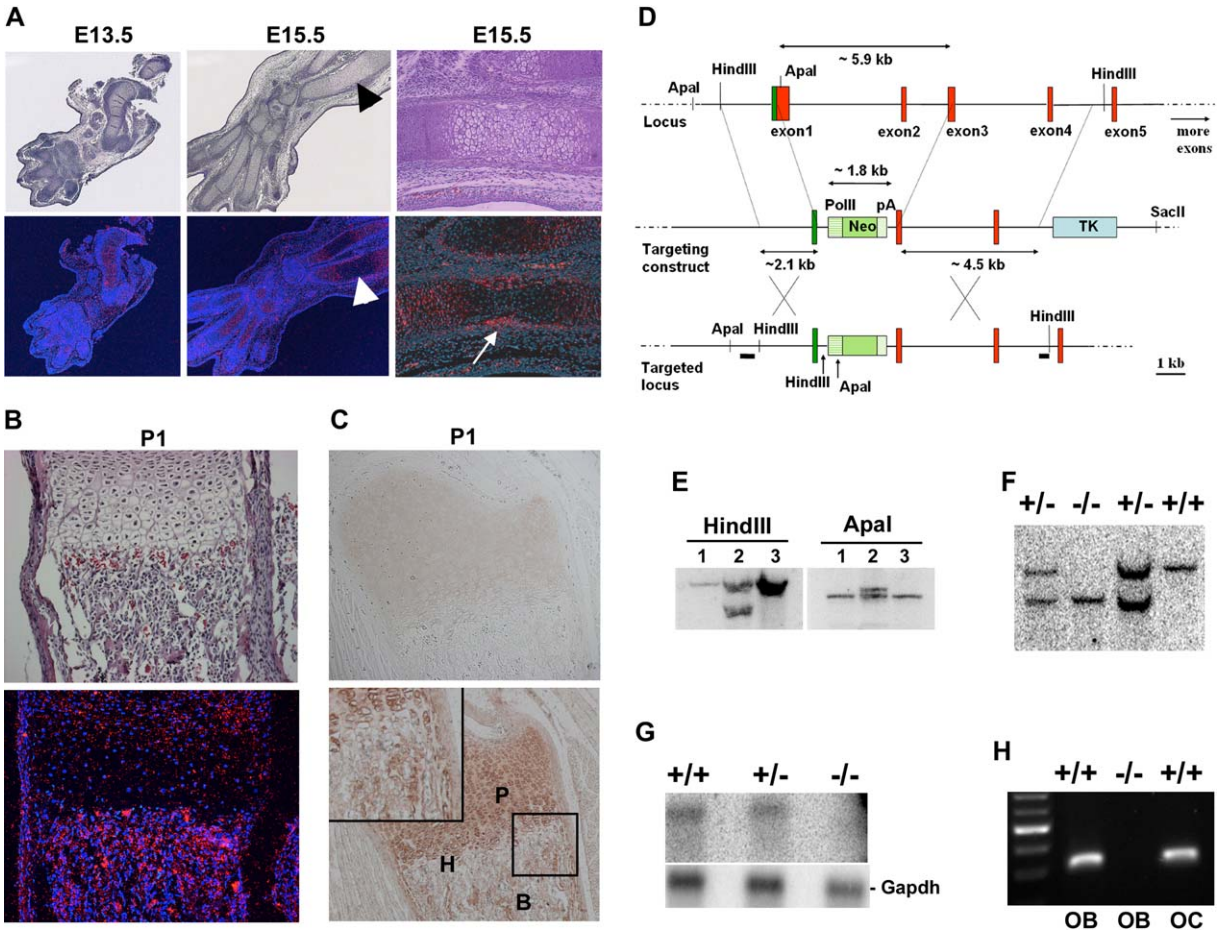

Figure 1. *Crtap* Expression during Skeletal Development and Generation of *Crtap*−/− Mice

(A and B) Serial mouse-limb sections at different stages of development stained with H&E (upper panels) or hybridized to *Crtap* (lower panels). *Crtap* mRNA (red), localizes to areas of chondrogenesis and to sites of vascular invasion where bone collar has formed (arrow) at E15.5. Note low expression of *Crtap* in hypertrophic chondrocytes (arrowheads). At P1, *Crtap* also strongly localizes to primary and secondary spongiosa where active bone formation takes place.

(C) P1 mouse-femur sections stained with a CRTAP polyclonal antibody (lower panel) or preimmune serum (upper panel). CRTAP was localized to proliferating chondrocytes (P) and bone (B and inset) but not hypertrophic chondrocytes (H).

(D) Schematic diagram of the construct used to generate *Crtap* knockout mice.

(E) Southern blot of targeted ES cell clone (lane 2) versus WT clones (lanes 1 and 3) digested with the listed enzyme and hybridized with the 3′ or 5′-flanking probe, respectively.

(F) Southern-blot genotyping of pups generated by intercross of *Crtap*+/− mice.

(G) Northern blot showing decreased and absence of *Crtap* mRNA in heterozygous and null mice total embryo RNA, respectively. *Gapdh* hybridization is the control for loading.

(H) RT-PCR showing *Crtap* expression in WT osteoblasts (OB) and osteoclasts (OC) but absence in *Crtap*−/− OB.

volume/tissue volume (BV/TV), trabecular thickness (Tb.Th), and trabecular number (Tb.N), and increased trabecular separation (Tb.sp) (Figure 3A). Kinetic indices of bone formation revealed a reduced bone formation rate (BFR) due to a reduction in the mineral apposition rate (MAR). *Crtap* mutant mice have normal mineralizing surfaces (MS/BS) consistent with the normal osteoblast numbers that were observed along trabeculae (Figure 3B). Osteoblast proliferative indices determined ex vivo by BrdU staining of cultured calvarial osteoblasts were comparable to WT values (data not shown). Additionally, the osteoid was markedly reduced in toluidine blue- and Goldner-stained sections and by quantification of osteoid thickness, surface, and volume (Figure 3C). Osteoid thickness is determined by the rate of osteoid deposition by osteoblasts and the rate of osteoid mineralization. Mineralization lag time (Mlt) was decreased in mutant mice. Hence, osteoblasts are producing osteoid at a slower rate as suggested by low MAR, but the osteoid is also being mineralized at a faster rate than in WT controls, suggesting an inherent alteration in both the quantity and quality of the osteoid matrix.

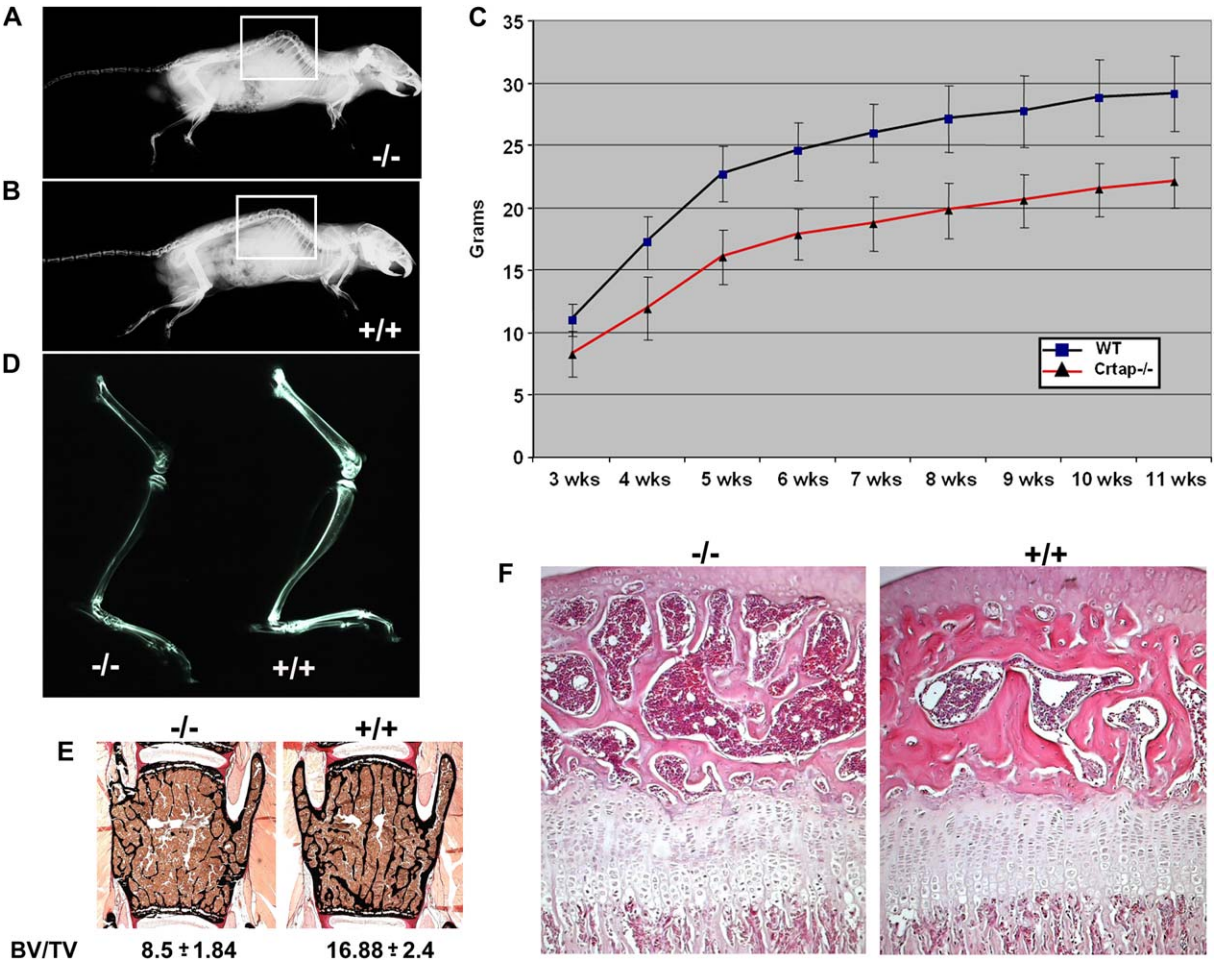

Figure 2. *Crtap*−/− Mice Are Smaller and Have Osteo-Chondrodysplasia, Kyphosis, and Severe Osteopenia Compared to WT Littermates

(A and B) Radiographs of 6-month old mice showing pronounced kyphosis (boxed) in *Crtap*−/− versus littermate control.

(C) Weight-curve analysis comparing *Crtap*−/− and WT male mice (mean ± SD, N = 10, $p < 0.01$) and female mice (N = 10, $p < 0.01$, data not shown).

(D) Rhizomelia and severe osteopenia are seen in this radiograph of a 6-week-old *Crtap*−/− versus control hind limb.

(E) L3 vertebral bodies from *Crtap*−/− and WT mice were embedded in methyl-methacrylate, sectioned, and stained with Von Kossa. BV/TV values shown are from 3-month-old male mice (mean ± SD, N = 6, $p < 0.01$).

(F) Comparison of 4-week-old proximal tibia sections from *Crtap*−/− and WT mice stained with H&E. Note thin trabeculae in the epiphyseal ossification center and dysplastic proliferating chondrocytes in *Crtap*−/− mice.

Because bone formation and resorption are coupled in vivo, we looked for an osteoclastic defect. The low bone mass in *Crtap*−/− mice, however, is likely not due to accelerated bone resorption since osteoclast numbers are normal in vivo (Figure S1), and ex vivo osteoclast function assessed by pit resorption and splenocyte differentiation was also normal (Figure S1). The absence of a hyperresorptive phenotype is supported by the finding of comparable urinary deoxypyridinoline (Dpd) levels in mutant versus WT mice (Figure 3D). Serum and urinary calcium, phosphorus, and magnesium were normal (data not shown), excluding a defect in mineral homeostasis. Hence, *Crtap* null mice exhibit a severe osteoporosis characterized by low bone mass, normal osteoblast and osteoclast numbers, reduced BFR/BS and MAR, and decreased osteoid synthesis and Mlt.

CRTAP Can Complex with Mammalian P3H1 and Is Required for Efficient 3-Hyp Modification of Fibrillar Collagen

Recently, it was shown that CRTAP copurified with Leprecan (P3H1) via gelatin sepharose chromatography in a screen to identify proteins that bound denatured collagens. However, CRTAP does not contain a 2-oxoglutarate dioxygenase domain and hence showed no collagen hydroxylation activity in vitro (Vranka et al., 2004). To determine if CRTAP can affect collagen prolyl 3-hydroxylation in vivo we analyzed collagens α1(I) and α1(II) chains for

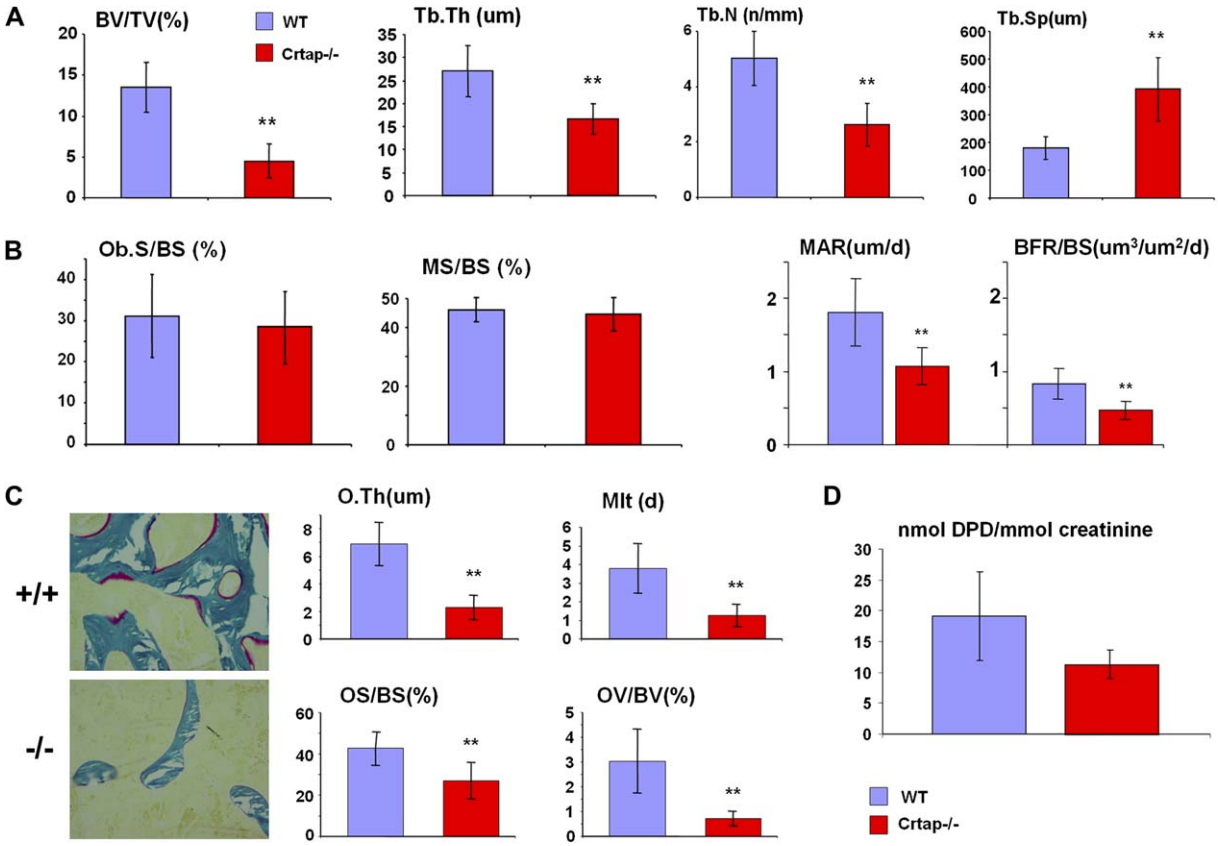

Figure 3. *Crtap*−/− Mice Have Functional Osteoblastic Defect and Decreased Osteoid

(A) Histomorphometric analyses of 3-month-old femurs show reduction in BV/TV, trabecular thickness, trabecular number, and increased trabecular separation (mean ± SD, N = 6, age and sex matched; **p < 0.01).

(B) While mineralizing and osteoblast surfaces were similar, the kinetic indices of bone formation, mineral apposition (MAR), and bone formation rates (BFR/BS) were significantly reduced in *Crtap*−/− versus controls (mean ± SD, N = 6, age and sex matched; **p < 0.01).

(C) Osteoid synthesis defect in *Crtap* null mice is demonstrated with Goldner staining (osteoid is stained in red). Osteoid measurements revealed decreased osteoid thickness (O.Th), osteoid surface (OS/BS), osteoid volume (OV/BV), and mineralization lag time (Mlt) in *Crtap*−/− versus controls (mean ± SD, N = 9, age matched; **p < 0.01).

(D) DPD analysis demonstrated comparable urine deoxypiridinoline levels in *Crtap*−/− versus control mice (mean ± SD, N = 6, females, 2–3 months old).

3-Hyp content in *Crtap*−/− and WT mice (Figure 4A). This was accomplished by resolving the cyanogen bromide (CNBr) peptides by SDS-PAGE followed by tandem mass spectrometric analyses of the trypsin digested, specific CNBr-peptide known to contain the 3-Hyp residue (Figure 4B). We found that α1(I) chains from bone and skin collagen and α1(II) chains from cartilage of mutant mice completely lacked the 3-hydroxyl modification at the single substrate proline residue near their carboxy terminus (Figure 4C and Figure S2). The SDS-PAGE results showed slight but significant slowing of the major cyanogen bromide (CB) peptides from cartilage type II collagen, suggesting overmodification of lysine residues (Figure 4B). These data indicate that prolyl 3-hydroxylation of fibrillar type I and II collagens is absent in *Crtap*−/− mice. To determine if collagen fibrils were altered structurally by loss of the prolyl 3-hydroxylation at this single residue in the triple-helical domain, we performed ultrastructural studies from mutant and WT mice. Collagen fibrils in mutant dermis and cartilage were thicker than in WT (skin [mean ± SD]: WT = 85 ± 7 nm versus mutant = 117 ± 9 nm, p < 0.0001; cartilage: WT = 85 ± 10 nm versus mutant = 117 ± 9 nm, p < 0.0001), suggesting that loss of this 3-Hyp residue may affect collagen fibril assembly (Figure 4D). To evaluate collagen intracellular processing, we performed collagen synthetic studies in mouse osteoblasts by steady state and pulse chase assays and found that type I procollagen chains were overmodified, based on a slower mobility, and, apparently, secreted in higher amount by *Crtap*−/− cells (Figures 4E and 4F). The latter was consistent with our observations on mutant primary calvarial osteoblasts in vitro, showing increased collagen staining (Van Gieson). Moreover, the in vivo observation of decreased mineralization lag time, i.e.,

A
N-term
Triple helix collagen domain
α1(I) -D GLN GLP GPI GPP GPR -
α1(II) -D GSN GIP GPI GPP GPR -
Unique 3-Hyp
B
Crtap
+/+ -/-
Crtap
+/+ -/-
CB6
CB9,7
Bone
Cartilage
C
α1(I) CB6 Tryptic Peptide
a) wt MS
782.0 [m+2H]2+
DGLNGLP*GPIGP#P*GPR
3-Hyp
[m+H]1+
1562.8
b) crtap MS
773.9 [m+2H]2+
DGLNGLP*GPIGPP*GPR
Pro
[m+H]1+
1546.8
c) wt MS2 782.0
DGLNGLP*GPIGP#P*GPR
d) crtap MS2 773.9
DGLNGLP*GPIGPP*GPR
Relative Abundance
m/z
D
+/+
-/-
E
-/- +/+ -/- +/+
– proα1(I)
– proα2(I)
α1(I) –
α2(I) –
DTT - +
Pepsin + -
F
+/+ -/-
0' 30' 60' 90' 0' 30' 60' 90'
[α1(III)]3 –
α1(I) –
α2(I) –
G
+/+ -/-
Van Gieson
Von Kossa
Mineralization nodules surface: 1.87% 7.32%

increased mineralization rate, correlated in vitro with the increased number of mineralization nodules in mutant versus control calvarial osteoblasts (Figure 4G). Hence, failure to 3-hydroxylate a single proline in fibrillar collagens I and II is associated with posttranslational overmodification, apparent altered rate of collagen production and matrix mineralization in osteoblasts, and increased fibril diameter.

Because collagen prolyl 3-hydroxylation takes place in the endoplasmic reticulum (ER), we determined the CRTAP subcellular localization. Immunofluorescence (IF) staining of Cos7, chick embryo chondrocytes (CEC), or MC615 cells transfected with an myc-tagged CRTAP expression construct showed a widespread and reticular pattern of distribution in the endoplasmic reticulum, with no nuclear staining. A partial colocalization with the Golgi was also observed, depending on the cell type that was examined; in particular, this was minimal or not detected in the mouse chondrocyte cell line MC615 (Figures 5A–5C).

Given the data indicating that CRTAP affects P3H1 function in vivo, we tested whether both proteins coexisted in a complex by subjecting gelatin binding protein fractions to velocity sedimentation on a sucrose gradient. P3H1 sediments to fractions 12/13, which also contain some CRTAP and Cyclophilin B (Figure S3A). Free CRTAP and Cyclophilin B sediment to fractions 19 and 23, respectively. The cosedimentation suggests that these proteins form a complex. This complex was isolated and analyzed by laser-light scattering. The molecular mass of the complex was 154.6 kDa (Figures 5D and 5E). This corresponds well to the calculated molecular mass of 155 kDa of a 1:1:1 complex of P3H1, CRTAP, and Cyclophilin B. Further in vitro evidence that P3H1 and CRTAP could directly interact came from Western analysis on affinity chromatography eluted proteins after binding to either CRTAP or P3H1 antibody columns. In both cases, using the appropriate antibody, we were able to detect the corresponding protein supporting that CRTAP and P3H1 can form a stable complex (Figures S3B and S3C).

Loss of *CRTAP* Is Associated with Recessive Osteogenesis Imperfecta

CRTAP maps to human chromosome 3p22.3 (Tonachini et al., 1999). Ward et.al. (2002) described a large consanguineous family in Quebec affected with a distinct ''rhizomelic'' form of osteogenesis imperfecta, termed OI type VII (Figure 6A) (Ward et al., 2002). This recessive form of OI was mapped to the short arm of chromosome 3 to a 5cM minimal interval localized between markers D3S2423 and D3S1561 (Labuda et al., 2002). This region contains 18 genes including *CRTAP* (Figure 6B). Given the rhizomelic osteochondrodysplastic phenotype of *Crtap* null mice, we hypothesized that CRTAP loss of function could cause OI VII. We found levels of *CRTAP* mRNA in cultured skin fibroblasts from two affected family members (patients IV-3 and V-7 of the Ward et al., 2002 pedigree) to be 10% those of four unrelated control subject cells after normalization to a single copy, constitutively expressed gene (β2-microglobulin) (Figure 6C, Table S1). Western blot analysis of patient and control fibroblast protein extracts showed decreased levels of CRTAP protein paralleling the change in mRNA (Figure 6D). The finding of residual normal-sized CRTAP suggested the possibility of a hypomorphic allele in this family. Sequence of the CRTAP coding and flanking intronic regions failed to identify a mutation, but all sites known to be polymorphic were homozygous in accordance with the consanguinity in this family.

RT-PCR amplification of RNA isolated from OI VII and control fibroblasts treated with and without cycloheximide demonstrated an additional longer CRTAP transcript in OI VII fibroblasts (Figure 6E). Sequence analysis of the longer transcript indicated the inclusion of 73 bp of intron 1. In *CRTAP* genomic DNA from an OI VII patient, we identified a single nucleotide change (c.472 −1021C>G) in intron 1 consistent with activation of a cryptic splice donor site and the inclusion of a 73 bp cryptic exon (position −1094 to −1021 5′ of exon 2) into the *CRTAP* cDNA (Figure 6F). This longer transcript contains a frame shift and is predicted to become degraded by the NMD

Figure 4. *Crtap*−/− α1(I) and α1(II) Collagens Lack the Unique 3-Hydroxyproline, Are Overmodified, and Form Fibrils with Increased Diameter

(A) Schematic diagram of a procollagen showing the 3-Hyp position in α1(I) and α1(II) collagens.

(B) Electrophoretic migration of cyanogen bromide-derived peptides generated from type I and type II collagens. CB peptides CB6 and CB9, seven containing the unique 3-Hyp residue, were analyzed by MS peptide mapping.

(C) The tryptic digest of α1(I)CB6 peptide was analyzed by tandem mass spectrometry. Top two panels (a, b) show the parent ions in the mass spectra from WT and *Crtap*−/− bone differing by 16 atomic mass units (1563 versus 1547) consistent with additional oxygen atom in WT peptides. Bottom two panels (c, d) show the MS/MS fragmentation spectra with daughter ions localizing the 16 mass difference to residues carboxy-terminal to the y6 position, consistent with absence of oxygen from $P^{\#}$ in the *Crtap*−/− peptide.

(D) Transmission electron micrographs show increased diameter in dermal fibroblast collagen fibrils from the *Crtap*−/− mice versus controls (magnification: ×72 K).

(E) Steady-state labeling of cultured primary calvarial mouse osteoblasts showing delayed migration of procollagen/collagen chains in *Crtap*−/− samples consistent with overmodification. Procollagen chains were precipitated from culture medium, +/− treatment with pepsin, and run on a 5% polyacrylamide-urea-SDS gel under reducing or nonreducing conditions, as indicated and repeated in two independent experiments.

(F) Collagen pulse-chase assays suggest increased rate of collagen secretion in mouse mutant osteoblasts versus WT controls. The medium fractions run on a 5% polyacrylamide-urea-SDS gel under nonreducing conditions are shown (the cell fraction gel is not shown). The experiment was normalized by total number of cells and repeated in three independent experiments.

(G) *Crtap*−/− primary calvarial osteoblasts cultured for 21 days in vitro show qualitative increase of collagen staining (Van Gieson) and number of mineralization nodules (Von Kossa) compared to WT controls (N = 3).

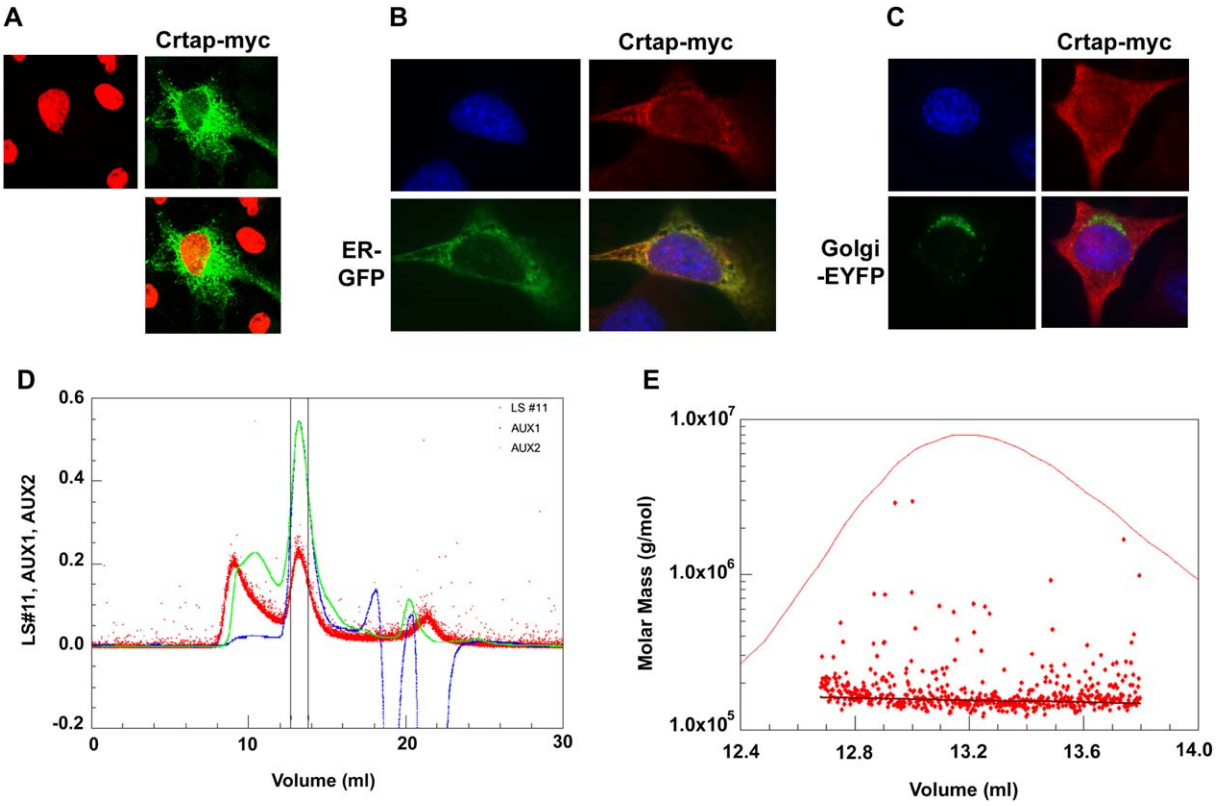

Figure 5. CRTAP Is Widely Localized in the Cell and Interacts with P3H1 in the rER

(A) Confocal microscopic image of Cos7 cells transfected with an myc-CRTAP construct and stained with anti-myc monoclonal antibody (green) showing a subcellular reticular pattern of expression. Nuclei were stained with propidium iodide (red).

(B) MC615 mouse chondrocyte cells were cotransfected with an myc-CRTAP construct (red) and an ER-targeted GFP (green) with Hoechst stained nuclei (blue). The merged image shows colocalization of CRTAP with the ER.

(C) MC615 cells were cotransfected with myc-CRTAP (red) and a Golgi-targeted EYFP (green) with Hoechst stained nuclei (blue). The merged image suggests no overlap between CRTAP and the Golgi.

(D) Fractions from the gelatin Sepharose column were run on a molecular sieve column attached to a laser-light scattering instrument. A peak at 155 kDa was found that contains P3H1. The elution profile of a fraction containing P3H1 on a Superose 12 column is shown. The light-scattering signal (red), refractive index signal (blue), and absorbance at 220 nm (green) are shown. Using the data of light scattered at multiple angles, one can determine the absolute mass, independently from the elution position of the column.

(E) The major peak (delineated by the two vertical bars in [D]) was analyzed by this method and the molar mass assessed. A molecular mass of 154.6 kDa was determined (black horizontal line).

mechanism. The point mutation in intron 1 was confirmed in four OI VII patients while the sequencing of eight unaffected members of the family showed that they were either carrier for the mutation (parents of affected) or WT (Figure S4).

To confirm that the decrease of *CRTAP* expression in OI VII patients translated to a biochemical alteration in fibrillar collagen, we performed a tandem mass spectrometry (MS/MS) analysis of trypsin-digested pepsinized collagen derived from the two patient versus control fibroblast-conditioned media. A significant (and variable) proportion of unhydroxylated Pro was found in patients but not in control cell medium collagen (Figure 6G). An identical result was seen in type I collagen extracted from an OI VII bone sample compared to unrelated controls (data not shown). Together, these findings strongly indicate that hypomorphic loss of function of *CRTAP* causes OI type VII.

This evidence led us to ask if a more severe human OI phenotype would be caused by complete loss of function of *CRTAP*. Such a mechanism would likely be found in pedigrees with recurrence of severe OI in children born to unaffected parents and associated with collagen overmodification. Until now, these cases had been attributed to either germline mosaicism and/or inheritance of an unknown recessive mutation. We studied one such consanguineous family in which four pregnancies were affected with short limbs and multiple fractures (Figure 7A). The diagnosis of recurrent OI type II was made based on the clinical features and the biochemical finding of type I collagen overmodification. However, *COL1A1* or *COL1A2* mutations could not be identified. Sequence analysis of *CRTAP* coding regions from probands VIII-3, VIII-5, and VIII-12 DNAs detected a homozygous single base pair (T) deletion in exon 4 (c.879delT). This deletion causes a frameshift

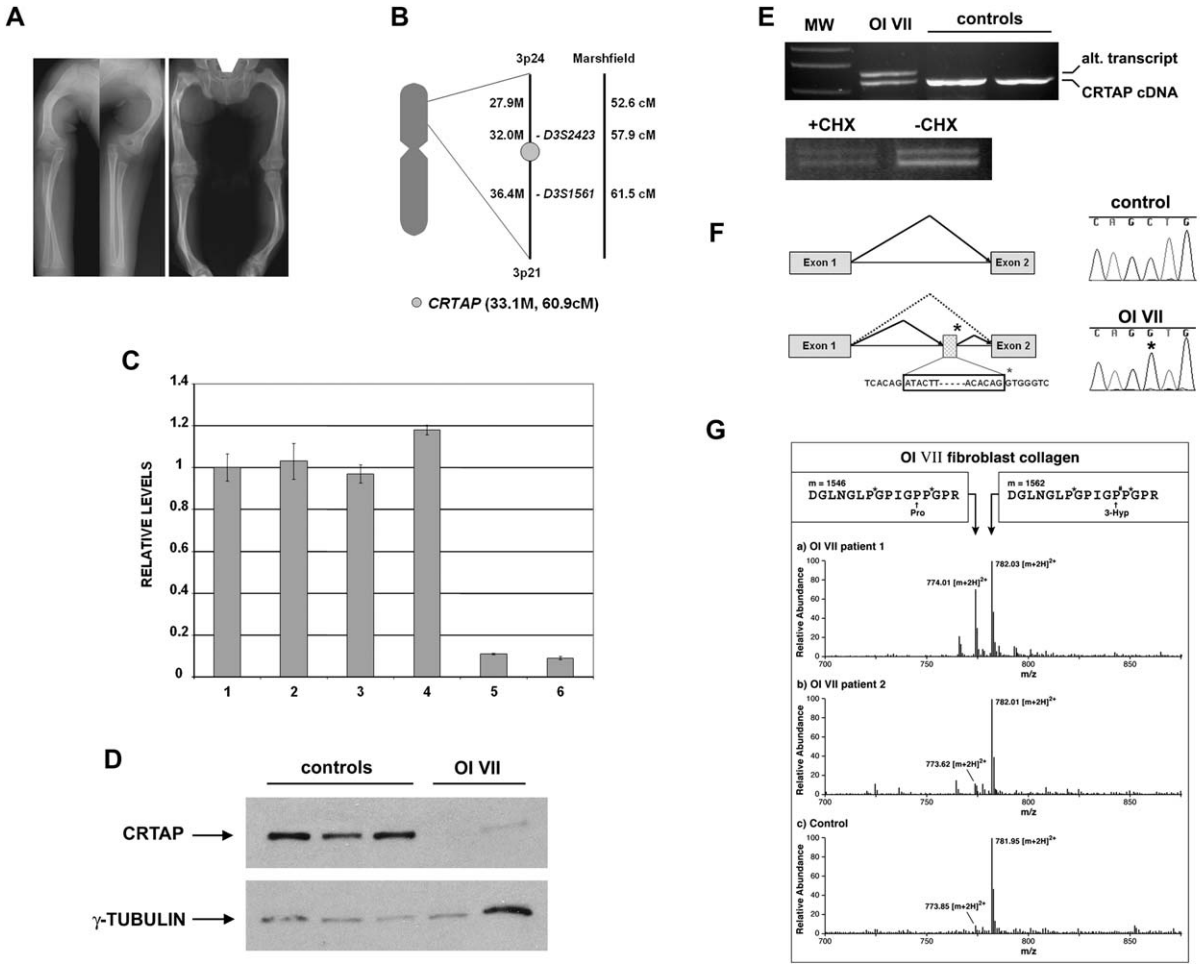

Figure 6. A *CRTAP* Splice Mutation Causes OI Type VII

(A) Left panels show upper extremity radiographs of a 2.5-year-old girl with OI type VII, showing selective shortening of the humeri (rhizomelia) and bowing deformity. Right panel shows lower extremity radiograph of the same patient, showing bilateral coxa vara and bowing deformity.

(B) Schematic diagram of human chromosome 3 with *CRTAP* localization within the 5cM OI VII critical region defined by the markers D3S2324 and D3S1561.

(C) Q-PCR analysis demonstrates levels of *CRTAP* mRNA in two OI VII patients (5 and 6) to be about 10% those of controls (1–4) (mean ± SD, three experiments).

(D) Western blot of fibroblast lysates shows decreased levels of CRTAP protein in OI VII samples normalized to γ-tubulin. Residual protein is detectable in patients when the lysate is overloaded (far right lane).

(E) PCR amplification of the exons 1–4 of *CRTAP* cDNA from OI VII and control fibroblasts treated with and without cycloheximide. An additional, longer transcript in the OI VII cells suggests the presence of a splice mutation. Proportion of mutant species is increased relative to WT in OI VII cells treated with cycloheximide (MW = molecular weight standards).

(F) Diagram showing the single base change (asterisk) in intron 1 (C>G) that generates a novel splice donor site. Utilization of an upstream acceptor site results in the inclusion of a cryptic 73 bp exon into the *CRTAP* mRNA. The longer transcript contains a frameshift with a stop codon 12 amino acids downstream of exon 1.

(G) Mass spectrometric analyses of pepsinized α1(I) collagen extracted from patient and control fibroblast-conditioned media show evidence of under-3-hydroxylation of proline in OI VII α1(I) chains. Residual and variable levels of 3-Hyp in the two patient samples is consistent with the proposed hypomorphic nature of this mutation.

with a premature termination codon 15 amino acids downstream and would be expected to cause a null allele due to nonsense-mediated decay. The parents of VIII-3 and VIII-5 (VII-1, VII-2) were asymptomatic but were carriers for the deletion (Figure 7A). Biochemical and MS/MS analysis of collagen from cultured fibroblasts from the proband confirmed collagen overmodification and showed that the target proline was underhydroxylated (Figure 7B). CRTAP protein could not be identified in fibroblasts from VIII-12 (Figure 7C). Finally, real-time PCR performed on RNA extracted from cultured fibroblasts showed that they contained 10% of the amount seen in the OI type VII cells and about 1% of that seen in control cells (Figure 7D, Table S1).

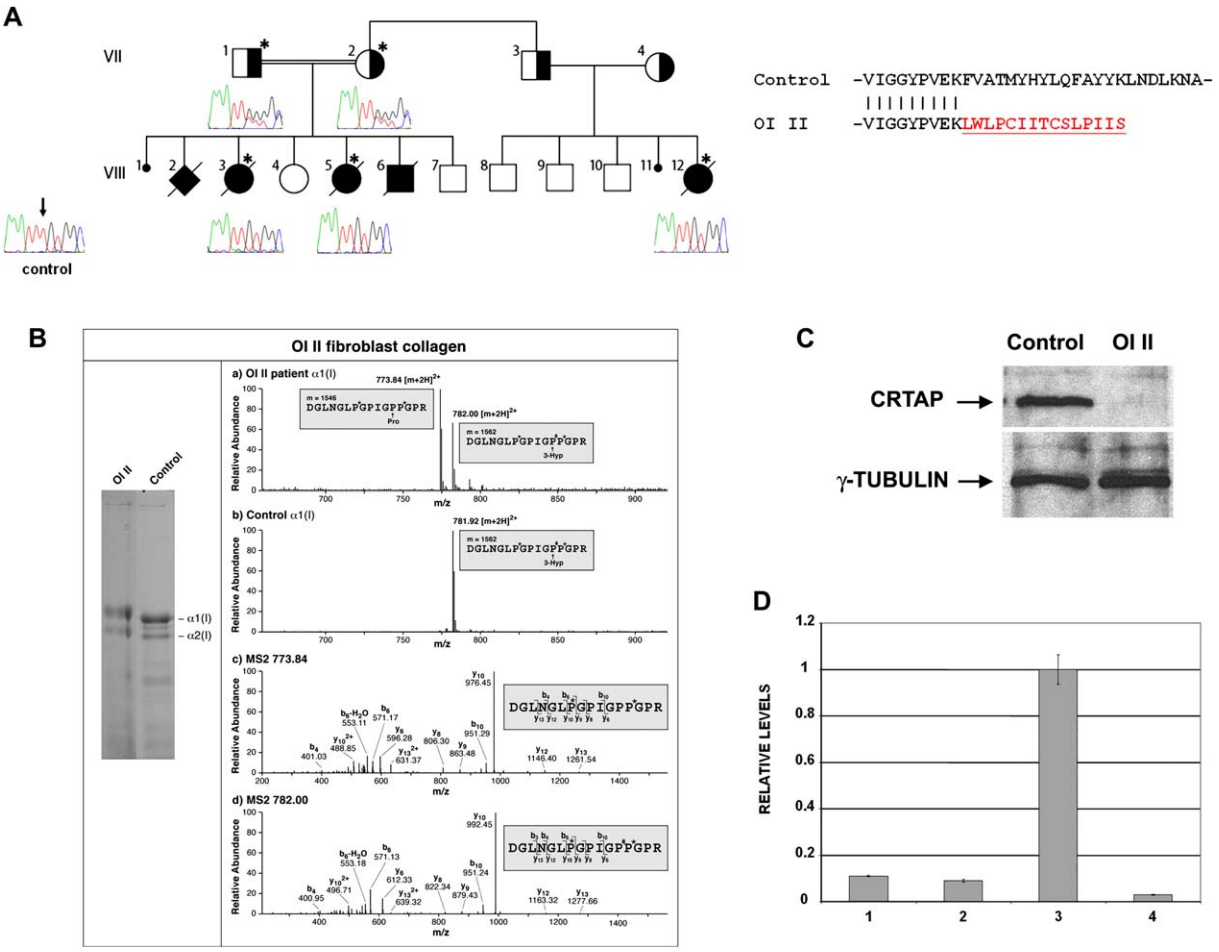

Figure 7. Loss of Function of *CRTAP* in Severe OI Type II

(A) Pedigree of an eight generation, consanguineous family (only the last two generations are depicted) showing multiple affected individuals with short limbs and multiple fractures and diagnosis of severe OI type II. Homozygous single base pair (T) deletion in *CRTAP* exon 4 was found in affected patients including VIII-3, VIII-5, and VIII-12. Unaffected parents (VII-1 and VII-2) were carriers for the mutation.

(B) Electrophoretic and MS/MS analyses of pepsinized medium collagen from OI II patient fibroblasts confirmed overmodification (left panel) and about 40% residual 3-Hyp compared to control.

(C) Western blot analysis revealed complete absence of CRTAP protein in fibroblast lysate from an OI II patient (VIII-12) versus control.

(D) Real time q-PCR demonstrated levels of *CRTAP* mRNA in OI II (4) that were 1% compared to normal control (3) and 10% of the OI VII (1–2) fibroblasts (Mean ± SD, three experiments).

Together, these data support that loss of function of *CRTAP* in humans is associated with a clinical spectrum of recessive OI. At the milder end of the spectrum, the clinical picture is one of bone fragility and rhizomelia seen in OI type VII; at the severe end, the phenotype is similar to lethal OI type II.

DISCUSSION

Prolyl 3-hydroxylation (Majamaa, 1981; Risteli et al., 1977; Tryggvason et al., 1979) has been a poorly understood collagen posttranslational modification. It occurs in fibril-forming type I and II collagens uniquely, at only one proline residue in the α1 chains (residue 986 of the triple-helical domain) but more frequently in network-forming type IV collagen. We show that loss of *Crtap* causes an osteochondrodysplasia characterized by short stature, kyphosis, and severe osteoporosis in mice. CRTAP can bind P3H1, and although the binding is not essential for enzymatic activity of P3H1 in vitro, CRTAP appears to be necessary for efficient 3-hydroxylation of fibrillar collagen prolyl residues in vivo. This could be due to its facilitation of P3H1 association with nascent procollagen chains. In humans, 10% residual CRTAP results in a rhizomelic form of recessive OI, while complete loss of the protein leads to a more severe form of OI. In both instances, the loss of protein is associated with marked decrease in 3-hydroxylation of the target prolyl residue in the triple-helical domain of type I collagen molecules.

CRTAP can form a complex with P3H1 in the rER where they can bind to pro-α collagen chains to mediate this post-translational modification. The major effects of CRTAP loss of function are on collagen modification, intracellular trafficking, and extracellular fibril assembly. The end result of these abnormalities is a functional defect in osteoid production and mineralization rate. Collagen overmodification usually reflects a delay in triple-helix formation, and this suggests a function for CRTAP and/or 3-Hyp in the regulation of collagen triple-helical assembly within the cell. The increased collagen fibril diameter outside of the cell and decreased osteoid volume and thickness in bone suggest that there is decreased deposition of osteoid. This may in part be due to inefficient fibril formation in the face of perhaps even increased procollagen secretion. The low osteoid thickness and MAR in the presence of normal numbers of osteoblasts support our conclusion that the net amount of bone matrix produced by these cells is abnormally low. The low Mlt suggests that the osteoid produced is mineralized in an abnormally fast manner. These effects, together, cause a severe low bone-mass phenotype that partially mimics observations made in children with OI (Rauch et al., 2000). Bone resorptive activity, however, was not increased in *Crtap* deficient mice. Thus, the findings suggest that the osteoporosis of these mice is due to deficient bone formation.

In addition to its important structural functions, type I collagen serves as a critical component in maintaining interactions with cell surfaces, other ECM molecules, and growth and differentiation factors. Over 50 molecules interact with type I collagen and many of the over 300 human mutations that have been reported in type I collagen genes affect sequences that are in these interaction domains (Di Lullo et al., 2002). For example, differential prolyl 4-hydroxylation of the collagen GXPGER sequence (which may occur in forms of OI with collagen overmodification) has been shown to affect collagen binding specificity to cell surface α1β1 versus α2β1 integrin (White et al., 2004). In a similar fashion, loss of 3-Hyp and/or CRTAP may also lead to dysregulation of specific collagen interactions.

CRTAP is related to the *P3H1*, *P3H2*, and *P3H3* family of genes and shares a tetratricopeptide-like domain located at their amino-terminal portions. P3H1 is localized specifically to tissues that express fibrillar collagen, suggesting that other P3H family members may be responsible for modifying basement membrane collagens. Hence, *CRTAP* may have diverse functions in multiple tissues related to prolyl 3-hydroxylation but also perhaps independent of this process.

Our data indicate that a quantitative defect in *CRTAP* causes OI type VII. In this case, an intronic mutation is associated with activation of a cryptic splice site, leading to generation of a longer transcript with a translational frameshift. This altered splicing occurs in most transcripts, as shown by 10% residual normal *CRTAP* mRNA and protein in patient fibroblasts. The clinical description of this condition as a "rhizomelic" form of OI correlates well with a function for *CRTAP* in cartilage and in bone. Instead, complete absence of CRTAP as a result of a frameshift that leads to NMD in all transcripts gives rise to a far more dramatic phenotype that is similar to a much more severe and potentially lethal form of OI. Thus, variable CRTAP loss of function is a mechanism for recessive OI and may contribute to a proportion of apparent de novo cases whose previous diagnosis was solely based on biochemical alterations in type I collagen. Traditionally, the recurrence risk assigned to unaffected parents who have a child with biochemically proven OI is quoted as up to 2% because of germline mosaicism (Cohn et al., 1990; Pepin et al., 1997). Our data suggest that in some instances, the diagnosis of OI secondary to the finding of classical type I collagen overmodification in cultured fibroblasts is due to recessive mutations in *CRTAP* with a recurrence risk of 25%. Moreover, our data suggest that there may be as yet undescribed connective tissue disease phenotypes that are due to dysregulation of prolyl 3-hydroxylation in other collagens, e.g., types III, IV, and V collagens. Such conditions might present a clinical spectrum more related to Ehlers Danlos syndrome (collagen III and/or V) and Alport syndrome (collagen IV). Finally, loss of the enzymatic activity of P3H1 might mimic loss of CRTAP, while the effects of mutations in CYPB remain to be explored.

EXPERIMENTAL PROCEDURES

ISH, Immunohistochemistry (IHC), IF, and Western Blot

ISH on paraffin-embedded tissues was performed as described previously (Morello et al., 2001). The *Crtap* RNA in situ probe contains the full-length open-reading frame (Morello et al., 1999). IHC analysis was performed with anti-CRTAP antisera as described elsewhere (Castagnola et al., 1997). Cell transfection, fixation, permeabilization, and IF procedures were performed as previously described (Tonachini et al., 2004). The myc-tagged CRTAP cDNA was inserted into pcDNA3.1 myc/his (Invitrogen). ER- and Golgi-targeted fluorescent GFP and EYFP constructs were from BD Clontech. MC615 cells (Mallein-Gerin and Olsen, 1993) were transfected with Fugene6 according to manufacturer's instructions (Roche). Alexa594 or Oregon Green514-conjugated goat anti-mouse antibody (Invitrogen) were used to detect the anti c-*myc* 9E10 monoclonal antibody (Evan et al., 1985) and nuclei were stained with Hoechst 33258 or with propidium iodide. Images were acquired with either a FV500 confocal microscope (Olympus) or with an Axiovert 200M (Zeiss). Western blots were performed using an anti-CRTAP polyclonal antibody and normalized with anti- γ-tubulin mouse monoclonal antibody (Sigma).

Targeting, Southern Blot, Northern Blot, RT-PCR, and Quantitative PCR (Q-PCR)

The *Crtap* targeting vector (shown in Figure 1) was electroporated into AB2.2 embryonic stem (ES) cells. Homologous recombination was identified by Southern analysis. Germ-line transmission of the mutant allele into C57BL6 was obtained. For Northern blot and RT-PCR, total RNA was extracted from tissues or cells using Trizol reagent (Invitrogen). Osteoclast RNA was a gift of Florent Elefteriou (UTHSC, San Antonio, TX). The Northern was probed with the same *Crtap* probe used for ISH. cDNA synthesis was performed using the SuperScript III First Strand RT-PCR kit (Invitrogen). Q-PCR was performed as described in the Supplemental Data.

Fibroblast Cultures and DNA Sequencing

Unrelated control fibroblasts used for Western, real-time, and RT-PCR experiments were primary human skin fibroblasts that matched the OI VII/II skin fibroblasts passage number and were fully comparable. They were grown in DMEM, 10% FBS. When indicated, cycloheximide (100 μg/ml) was added for 5 hr and then RNA and cDNA were prepared as described above. Patient samples were PCR amplified using intron-specific primers and directly sequenced with dye terminator chemistry. Single nucleotide polymorphisms were compared with the Weizmann Institute of Science database (www.genecards.org). *CRTAP* mutations are described with the Ensembl gene ID ENSG00000170275 as the reference sequence.

Clinical Data

The OI type II family (Figure 7A) is of Indian descent, and the parents of the proband (VIII-3) are second cousins but also related by a more complex consanguinity loop with common ancestors seven generations back. The first pregnancy was a spontaneous loss and the second (VIII-2) was found to have very short limbs with multiple fractures at 16 weeks gestation, consistent with OI type II. The third pregnancy was terminated at 16 weeks for the same findings, and cells grown from skin of that fetus synthesized abnormal type I procollagen, in which all chains were overmodified. Sequence of the cDNAs from *COL1A1* and *COL1A2* were normal. Cells from VIII-5 and VIII-6 all made overmodified type I procollagen molecules. The family had two unaffected children. Four years after the birth of VIII-6, the mother's brother (VII-3) and his wife (VII-4) had an affected pregnancy (ultrasound examination) that was terminated.

Radiographs, Bone Histology/Histomorphometry, and Tissue Staining

Radiographs were obtained by Faxitron (Faxitron X-ray Corp., Wheeling, IL). Routine histologic analysis of paraffin-embedded long bone and growth plates was done as per standard protocols. Histomorphometric analysis of static and dynamic parameters (using 20 mg/kg calcein injection) of bone resorption, formation, and volume was carried out according to standard procedures (Parfitt et al., 1987) in 12 week-old *Crtap*−/− and WT mice (N = 6 each sex and genotype) proximal tibial secondary spongiosa using the Osteomeasure image analysis system (OsteoMetrics, Inc., Decatur, GA). Goldner and Von Kossa staining were performed using standard protocols.

Collagen Studies and Mass Spectrometry

Collagen steady-state and pulse-chase assays were performed as described (Bonadio et al., 1985; Kuznetsova et al., 2004). Primary calvarial osteoblasts were labeled with 70 μCi of L-[2,3,4,5-^{3}H] proline. For pulse-chase assays, cells were labeled for 4 hours and then chased with fresh medium containing cold proline at time 0. Both medium and cell layer were harvested at 30′ intervals and analyzed separately. Collagens were obtained by overnight pepsin digestion (55 μg/ml) of procollagen samples.

For quantification of 3-Hyp in collagen preparations obtained from tissues or skin fibroblast cultures, CNBR-derived peptides (CB peptides) or pepsinized collagens were isolated and tryptic digests prepared for MS/MS. See Supplemental Data for mass spectrometry conditions. Transmission electron microscopy was performed on skin and sternal cartilage biopsies from WT and mutant mice (N = 3). The fibril diameter of ten fibrils in each of five different areas per mouse was measured (N = 150 total measurements each genotype).

Affinity Column Purification, Velocity Sedimentation, Laser-Light Scattering

For affinity column purification and velocity sedimentation, see Supplemental Data.

P3H1 associations, based on the measured molar masses, were observed using a multi-angle light scattering (MALS) instrument (DAWN Eos, Wyatt Technology). The instrument was placed in line with a UV detector, refractive index detector (RI, Wyatt), and a quasi-elastic light scattering detector (QELS, Wyatt) during size-exclusion chromatography (SEC). SEC was performed with a Superose 12 10/300 GL column (Amersham Biosciences) equilibrated in phosphate-buffered saline with a flow rate of 0.2 ml/min. Signals from the UV, RI, and MALS detectors were normalized using bovine serum albumin. Monodisperse regions under the peak were analyzed. The weight-averaged molar masses (M_w) were reported based on the average protein concentration for the peak area analyzed. The peak area analyzed was approximately 75%.

DPD Assay, Osteoblasts, and Osteoclasts In Vitro Studies

The deoxypyridinoline crosslinks (DPD) assay for free DPD was performed using a Metra DPD EIA kit (Quidel) according to manufacturer's instructions, and results were normalized to creatinine levels (Creatinine Assay kit, Quidel). In vitro cultures of primary osteoblasts (N = 3) from P4 mice were established as previously described (Kuznetsova et al., 2004). Van Gieson and Von Kossa staining were performed according to standard protocols. Osteoclasts were generated from splenocytes with M-CSF and RANKL (10 ng/ml), stained for TRAP activity, and counted, as described previously (Xing et al., 2002).

Statistical Analyses

Data are expressed as mean values ± standard deviation (SD). Statistical significance was computed using the Student's t test. A P value < 0.05 was considered statistically significant.

Supplemental Data

Supplemental Data include four figures, one table, and experimental procedures and can be found with this article online at http://www.cell.com/cgi/content/full/127/2/291/DC1/.

ACKNOWLEDGMENTS

We thank Dr. Millan Patel for helpful discussions, Dr. Mallein-Gering for kindly providing the MC615 cell line, and Raffaela Arbicò for expert technical assistance. The monoclonal antibody 9E10 was obtained from the Developmental Studies Hybridoma Bank developed under the auspices of the NICHD and maintained by the University of Iowa, Dept. of Biological Sciences, Iowa City, IA. This work was supported by NIH grants DE01771 (B.L.), ES11253 (B.L.), HD22657 (B.L., D.E.), AR43510 (B.B.), AR051459 (R.M.), AR37318 (D.E.), AR41223 (P.B.), the Baylor College of Medicine Mental Retardation Developmental Disabilities Research Center (MRDDRC), the Shriners of North America (H.P.B., F.H.G.), and the Osteogenesis Imperfecta Foundation and the Bone Disease Program of Texas (R.M.).

Received: January 31, 2006
Revised: May 4, 2006
Accepted: August 18, 2006
Published: October 19, 2006

REFERENCES

Andrade, M.A., Perez-Iratxeta, C., and Ponting, C.P. (2001). Protein repeats: structures, functions, and evolution. J. Struct. Biol. *134*, 117–131.

Aravind, L., and Koonin, E.V. (2001). The DNA-repair protein AlkB, EGL-9, and leprecan define new families of 2-oxoglutarate- and iron-dependent dioxygenases. Genome Biol. *2*, RESEARCH0007.

Berg, R.A., and Prockop, D.J. (1973a). Purification of (14C) protocollagen and its hydroxylation by prolyl-hydroxylase. Biochemistry *12*, 3395–3401.

Berg, R.A., and Prockop, D.J. (1973b). The thermal transition of a non-hydroxylated form of collagen. Evidence for a role for hydroxyproline in stabilizing the triple-helix of collagen. Biochem. Biophys. Res. Commun. *52*, 115–120.

Bonadio, J., Holbrook, K.A., Gelinas, R.E., Jacob, J., and Byers, P.H. (1985). Altered triple helical structure of type I procollagen in lethal perinatal osteogenesis imperfecta. J. Biol. Chem. *260*, 1734–1742.

Byers, P.H., and Cole, W.G. (2002). Osteogenesis Imperfecta. In Connective Tissue and Heritable Disorders Second Edition, P.M. Royce and B. Steinmann, eds. (New York: Wiley-Liss), pp. 285–430.

Castagnola, P., Gennari, M., Morello, R., Tonachini, L., Marin, O., Gaggero, A., and Cancedda, R. (1997). Cartilage associated protein (CASP) is a novel developmentally regulated chick embryo protein. J. Cell Sci. *110*, 1351–1359.

Cohn, D.H., Starman, B.J., Blumberg, B., and Byers, P.H. (1990). Recurrence of lethal osteogenesis imperfecta due to parental mosaicism for a dominant mutation in a human type I collagen gene (COL1A1). Am. J. Hum. Genet. *46*, 591–601.

Di Lullo, G.A., Sweeney, S.M., Korkko, J., Ala-Kokko, L., and San Antonio, J.D. (2002). Mapping the ligand-binding sites and disease-associated mutations on the most abundant protein in the human, type I collagen. J. Biol. Chem. *277*, 4223–4231.

Dreyer, S.D., Zhou, G., and Lee, B. (1998). The long and the short of it: developmental genetics of the skeletal dysplasias. Clin. Genet. *54*, 464–473.

Evan, G.I., Lewis, G.K., Ramsay, G., and Bishop, J.M. (1985). Isolation of monoclonal antibodies specific for human c-myc proto-oncogene product. Mol. Cell. Biol. *5*, 3610–3616.

Eyre, D.R. (2004). Collagens and cartilage matrix homeostasis. Clin. Orthop. Relat. Res. *427*, S118–S122.

Glorieux, F.H., Rauch, F., Plotkin, H., Ward, L., Travers, R., Roughley, P., Lalic, L., Glorieux, D.F., Fassier, F., and Bishop, N.J. (2000). Type V osteogenesis imperfecta: a new form of brittle bone disease. J. Bone Miner. Res. *15*, 1650–1658.

Glorieux, F.H., Ward, L.M., Rauch, F., Lalic, L., Roughley, P.J., and Travers, R. (2002). Osteogenesis imperfecta type VI: a form of brittle bone disease with a mineralization defect. J. Bone Miner. Res. *17*, 30–38.

Hyland, J., Ala-Kokko, L., Royce, P., Steinmann, B., Kivirikko, K.I., and Myllyla, R. (1992). A homozygous stop codon in the lysyl hydroxylase gene in two siblings with Ehlers-Danlos syndrome type VI. Nat. Genet. *2*, 228–231.

Jenkins, C.L., Bretscher, L.E., Guzei, I.A., and Raines, R.T. (2003). Effect of 3-hydroxyproline residues on collagen stability. J. Am. Chem. Soc. *125*, 6422–6427.

Kaul, S.C., Sugihara, T., Yoshida, A., Nomura, H., and Wadhwa, R. (2000). Gros1, a potential growth suppressor on chromosome 1: its identity to basement membrane-associated proteoglycan, leprecan. Oncogene *19*, 3576–3583.

Kefalides, N.A. (1973). Structure and biosynthesis of basement membranes. Int. Rev. Connect. Tissue Res. *6*, 63–104.

Kresina, T.F., and Miller, E.J. (1979). Isolation and characterization of basement membrane collagen from human placental tissue. Evidence for the presence of two genetically distinct collagen chains. Biochemistry *18*, 3089–3097.

Kuznetsova, N.V., Forlino, A., Cabral, W.A., Marini, J.C., and Leikin, S. (2004). Structure, stability and interactions of type I collagen with GLY349-CYS substitution in alpha 1(I) chain in a murine Osteogenesis Imperfecta model. Matrix Biol. *23*, 101–112.

Labuda, M., Morissette, J., Ward, L.M., Rauch, F., Lalic, L., Roughley, P.J., and Glorieux, F.H. (2002). Osteogenesis imperfecta type VII maps to the short arm of chromosome 3. Bone *31*, 19–25.

Lamande, S.R., and Bateman, J.F. (1999). Procollagen folding and assembly: the role of endoplasmic reticulum enzymes and molecular chaperones. Semin. Cell Dev. Biol. *10*, 455–464.

Lee, B., Vissing, H., Ramirez, F., Rogers, D., and Rimoin, D. (1989). Identification of the molecular defect in a family with spondyloepiphyseal dysplasia. Science *244*, 978–980.

Majamaa, K. (1981). Effect of prevention of procollagen triple-helix formation on proline 3-hydroxylation in freshly isolated chick-embryo tendon cells. Biochem. J. *196*, 203–206.

Mallein-Gerin, F., and Olsen, B.R. (1993). Expression of simian virus 40 large T (tumor) oncogene in mouse chondrocytes induces cell proliferation without loss of the differentiated phenotype. Proc. Natl. Acad. Sci. USA *90*, 3289–3293.

Mizuno, K., Hayashi, T., Peyton, D.H., and Bachinger, H.P. (2004). The peptides acetyl-(Gly-3(S)Hyp-4(R)Hyp)10-NH2 and acetyl-(Gly-Pro-3(S)Hyp)10-NH2 do not form a collagen triple helix. J. Biol. Chem. *279*, 282–287.

Morello, R., Tonachini, L., Monticone, M., Viggiano, L., Rocchi, M., Cancedda, R., and Castagnola, P. (1999). cDNA cloning, characterization and chromosome mapping of Crtap encoding the mouse cartilage associated protein. Matrix Biol. *18*, 319–324.

Morello, R., Zhou, G., Dreyer, S.D., Harvey, S.J., Ninomiya, Y., Thorner, P.S., Miner, J.H., Cole, W., Winterpacht, A., Zabel, B., et al. (2001). Regulation of glomerular basement membrane collagen expression by LMX1B contributes to renal disease in nail patella syndrome. Nat. Genet. *27*, 205–208.

Myllyharju, J. (2003). Prolyl 4-hydroxylases, the key enzymes of collagen biosynthesis. Matrix Biol. *22*, 15–24.

Myllyharju, J., and Kivirikko, K.I. (2004). Collagens, modifying enzymes and their mutations in humans, flies and worms. Trends Genet. *20*, 33–43.

Parfitt, A.M., Drezner, M.K., Glorieux, F.H., Kanis, J.A., Malluche, H., Meunier, P.J., Ott, S.M., and Recker, R.R. (1987). Bone histomorphometry: standardization of nomenclature, symbols, and units. Report of the ASBMR Histomorphometry Nomenclature Committee. J. Bone Miner. Res. *2*, 595–610.

Pepin, M., Atkinson, M., Starman, B.J., and Byers, P.H. (1997). Strategies and outcomes of prenatal diagnosis for osteogenesis imperfecta: a review of biochemical and molecular studies completed in 129 pregnancies. Prenat. Diagn. *17*, 559–570.

Pihlajaniemi, T., Dickson, L.A., Pope, F.M., Korhonen, V.R., Nicholls, A., Prockop, D.J., and Myers, J.C. (1984). Osteogenesis imperfecta: cloning of a pro-alpha 2(I) collagen gene with a frameshift mutation. J. Biol. Chem. *259*, 12941–12944.

Rauch, F., Travers, R., Parfitt, A.M., and Glorieux, F.H. (2000). Static and dynamic bone histomorphometry in children with osteogenesis imperfecta. Bone *26*, 581–589.

Risteli, J., Tryggvason, K., and Kivirikko, K.I. (1977). Prolyl 3-hydroxylase: partial characterization of the enzyme from rat kidney cortex. Eur. J. Biochem. *73*, 485–492.

Semenza, G.L. (2001). HIF-1, O(2), and the 3 PHDs: how animal cells signal hypoxia to the nucleus. Cell *107*, 1–3.

Tonachini, L., Monticone, M., Puri, C., Tacchetti, C., Pinton, P., Rizzuto, R., Cancedda, R., Tavella, S., and Castagnola, P. (2004). Chondrocyte protein with a poly-proline region (CHPPR) is a novel mitochondrial protein and promotes mitochondrial fission. J. Cell. Physiol. *201*, 470–482.

Tonachini, L., Morello, R., Monticone, M., Skaug, J., Scherer, S.W., Cancedda, R., and Castagnola, P. (1999). cDNA cloning, characterization and chromosome mapping of the gene encoding human cartilage associated protein (CRTAP). Cytogenet. Cell Genet. *87*, 191–194.

Tryggvason, K., Majamaa, K., and Kivirikko, K.I. (1979). Prolyl 3-hydroxylase and 4-hydroxylase activities in certain rat and chick-embryo tissues and age-related changes in their activities in the rat. Biochem. J. *178*, 127–131.

Vranka, J.A., Sakai, L.Y., and Bachinger, H.P. (2004). Prolyl 3-hydroxylase *1*, enzyme characterization and identification of a novel family of enzymes. J. Biol. Chem. *279*, 23615–23621.

Ward, L.M., Rauch, F., Travers, R., Chabot, G., Azouz, E.M., Lalic, L., Roughley, P.J., and Glorieux, F.H. (2002). Osteogenesis imperfecta type VII: an autosomal recessive form of brittle bone disease. Bone *31*, 12–18.

Wassenhove-McCarthy, D.J., and McCarthy, K.J. (1999). Molecular characterization of a novel basement membrane-associated proteoglycan, leprecan. J. Biol. Chem. *274*, 25004–25017.

White, D.J., Puranen, S., Johnson, M.S., and Heino, J. (2004). The collagen receptor subfamily of the integrins. Int. J. Biochem. Cell Biol. *36*, 1405–1410.

Xing, L., Bushnell, T.P., Carlson, L., Tai, Z., Tondravi, M., Siebenlist, U., Young, F., and Boyce, B.F. (2002). NF-kappaB p50 and p52 expression is not required for RANK-expressing osteoclast progenitor formation but is essential for RANK- and cytokine-mediated osteoclastogenesis. J. Bone Miner. Res. *17*, 1200–1210.